Computer simulations predict that chromosome movements and rotations accelerate mitotic spindle assembly without compromising accuracy

Raja Paul[a,b], Roy Wollman[c], William T. Silkworth[d], Isaac K. Nardi[d], Daniela Cimini[d], and Alex Mogilner[a,b,1]

Departments of [a]Neurobiology, Physiology, and Behavior and [b]Mathematics University of California, Davis, CA 95616; [c]Department of Chemical and Systems Biology, Stanford University Medical Center, Stanford, CA 94305; and [d]Department of Biological Sciences, Virginia Polytechnic Institute and State University, Blacksburg, VA 24061

The mitotic spindle self-assembles in prometaphase by a combination of centrosomal pathway, in which dynamically unstable microtubules search in space until chromosomes are captured, and a chromosomal pathway, in which microtubules grow from chromosomes and focus to the spindle poles. Quantitative mechanistic understanding of how spindle assembly can be both fast and accurate is lacking. Specifically, it is unclear how, if at all, chromosome movements and combining the centrosomal and chromosomal pathways affect the assembly speed and accuracy. We used computer simulations and high-resolution microscopy to test plausible pathways of spindle assembly in realistic geometry. Our results suggest that an optimal combination of centrosomal and chromosomal pathways, spatially biased microtubule growth, and chromosome movements and rotations is needed to complete prometaphase in 10–20 min while keeping erroneous merotelic attachments down to a few percent. The simulations also provide kinetic constraints for alternative error correction mechanisms, shed light on the dual role of chromosome arm volume, and compare well with experimental data for bipolar and multipolar HT-29 colorectal cancer cells.

assembly speed and accuracy | merotelic attachments | microtubules | search and capture

Fig. 1. Computer model of spindle assembly. (*A*) MTs (growing in blue, shortening in red, captured in green) searching from two foci (centrosomes) for KTs (captured in green, not captured in blue) on the chromosomes (white/gray). (Scale bar, 2 mm.) (*B*) Four possible types of chromosome attachments. Amphitelic attachment: The two sister KTs are bound to MTs coming from opposite poles. Monotelic attachment: One sister KT is bound to MTs, whereas the other is unattached. Syntelic attachment: Both sister KTs are bound to MTs from the same spindle pole. Merotelic attachment: One KT is bound to MTs from opposite spindle poles.

The mitotic spindle is a complex molecular machine segregating chromosomes (1, 2). Molecular inventory and general principles of the spindle dynamics are becoming clear (3), but quantitative understanding of spindle mechanics in general and its self-assembly in particular is lacking. The first hypothesis of how the spindle assembles, elegantly called "search and capture" (Fig. 1*A*), was put forward in ref. 4 after the discovery of the dynamic instability phenomenon: Microtubules (MTs) grow and shorten rapidly and repeatedly from the centrosomes in random directions "searching" for the kinetochores (KTs), specialized chromosome structures that function as an interface between the chromosomes and the mitotic spindle. Whenever a growing MT plus end runs into a KT, this MT is stabilized; the assembly is complete when all KTs are thus captured transforming two MT asters into a typical bipolar spindle. Capture of a single astral MT by a KT has been visualized directly in newt lung cell cultures (5).

How can hundreds of MTs turning over in tens of seconds capture tens of chromosomes within 10–20 min (6) is one of the fundamental questions of mitosis. Mathematical modeling has been instrumental in attempts to answer this question, because it is very hard to experimentally resolve individual MTs, follow their formation, and perturb their dynamics (7). First applications of modeling were the analyses (8, 9) suggesting that the dynamic instability parameters have to be optimized to ensure fast assembly, so that a MT switches from growth to shortening when it is as long as the distance between the centrosome and the chromosome. This analysis was extended (10) to simulate hundreds of MTs searching for tens of KTs in realistic geometry. The simulations demonstrated that even optimally fine-tuned dynamic instability cannot explain the typical observed prometaphase duration of 10–20 min. How-
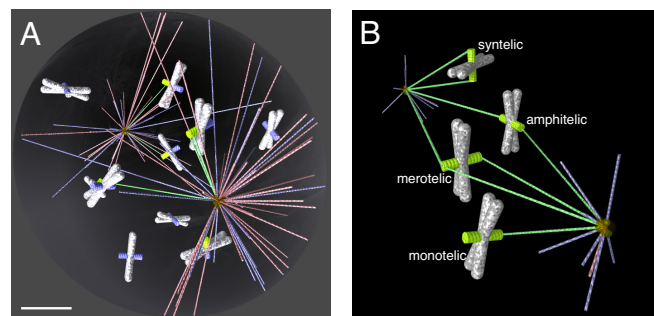
ever, a spatially biased search and capture process, in which the MTs grow without catastrophes within the nuclear sphere (i.e., volume through which chromosomes are distributed upon nuclear envelope breakdown) and catastrophe very fast away from it is predicted to be fast enough (10). The likely mechanisms for such spatial bias are the RanGTP gradient around the chromosomes (11, 12) and motor-dependent mechanisms (13, 14) locally regulating MT dynamics.

Three factors limit predictive power of our previous model (10). First, for technical reasons, the chromosome arms were "transparent" to the searching MTs, which led to overly optimistic predictions: MTs were able to search the whole nuclear space, although in reality, most of it is blocked by the chromosome arms. Second, the search-and-capture cannot explain mitosis in cells lacking centrosomes. In such cells, MTs are nucleated near the chromosomes, and then sorted into arrays with their minus ends extending outward, and finally focused at the minus ends as a result of complex activities of mitotic motors (15) establishing the spindle poles (16). It was thought that the centrosome-, and chromosome-directed pathways operate in different cells, but previously undiscovered data have demonstrated that centrosome-independent pathway occurs in cells that possess centrosomes (7) and that cells adopted

---

both pathways for spindle self-assembly (17). Namely, the astral, centrosome-nucleated MTs capture the bundles of the KT-nucleated MTs, rather than KTs themselves, and then integrate the centrosomal–chromosomal bundles into a spindle-like structure (7). Third, in our previous study (10), we were concerned only with the speed of spindle self-assembly, but the assembly also has to be accurate: Ideally, all chromosomal connections have to be correct amphitelic attachments, in which the two sister KTs on each chromosome are captured from the opposite spindle poles, but monotelic, syntelic, or merotelic attachments are also possible (Fig. 1B). Erroneous attachments exist in early mitosis (18, 19), but later, most of them are corrected (19–22). The questions about how many erroneous attachments would result from the search-and-capture process, what kind of correction mechanisms have to be deployed, and what are the kinetic constraints on such mechanisms were raised qualitatively (23, 24), but never examined quantitatively.

In this study, we explore computationally the simplest "stochastic/geometric" hypothesis of erroneous attachment formation (19, 23): Merotelic and syntelic attachments are established as errors inherent to the stochastic nature of the search-and-capture mechanism when one KT is "visible" from both spindle poles, so the MTs from the respective poles reach this KT almost simultaneously (merotely) or when sister KTs are visible from the same pole and, again, are captured from this pole at once (syntely). We estimated the number of such attachments and found it to be tremendous, exceeding by far the numbers observed experimentally. We therefore tested a number of potential error-correction mechanisms including MT turnover and chromosome turning after the first capture, and found stringent constraints on kinetics of these error-correction mechanisms. The simulations revealed that chromosomes also have to move rapidly to ensure timely spindle assembly. The model suggests that the finite chromosome volume plays a dual role, on the one hand hindering the assembly by shielding KTs at the center of the nucleus, but on the other hand accelerating MT cycles by promoting MT catastrophes. The simulations further illustrate that in the hybrid assembly pathway, the longer the chromosomal MT bundles are, the faster, but also less accurate, the assembly is, hinting that the cell has to optimize the MT dynamics to achieve the conflicting goals of efficiency (rapid assembly) and accuracy (minimizing number of erroneous attachments). We calibrated the model by quantifying prometaphase dynamics, timing, and spindle geometry in HT-29 colorectal cancer cells.

Model

We simulated vertebrate cells' spindle assembly in realistic 3D geometry (Fig. 1A). In the model, the chromosomes, KTs, and MTs are dynamic objects behaving according to computational rules inferred from cell biological hypotheses. The model rules and assumptions are: Each of two centrosomes placed at the opposite poles of the nuclear sphere's diameter anchor minus ends of 250 astral MTs. Each MT is a rod of zero thickness undergoing dynamic instability; its plus end grows steadily until a catastrophe occurs with a constant rate, upon which the MT shortens with a constant speed. While growing, the MT does not turn, and the new cycle starts with growth in a random direction. There are no MT rescues: We undertook exhaustive simulations that showed that the fastest capture occurs at zero rescue frequency, because when a MT grows with no KT on the growth path, rescues prolong such futile searches. We simulated both unbiased and biased searches. In the former, the constant catastrophe frequency is equal approximately to the MT growth rate divided by 85% of the nuclear sphere's diameter: At this frequency, a MT on average reaches the length optimal to reach the majority of KTs (10), yet does not waste time on longer cycles. In the latter, MTs are stable in the chromosomes' proximity and do not undergo any catastrophe events inside the nuclear sphere. Once a MT plus end goes beyond the volume of the nuclear sphere, it undergoes a catastrophe event and shrinks all the way back to the centrosome. In both scenarios, MTs start shortening immediately

upon a collision with a chromosome arm [see discussion in supporting information (SI) Text]. A MT plus end is instantly stabilized upon encountering a KT, and this KT is said to be captured. Upon such capture, a new dynamic MT replaces the stabilized one at the same pole.

Chromosomes are modeled as solid 3D cylinders that are uniformly randomly distributed within the nuclear sphere and oriented in random directions. In the static regime (Movie S1), the chromosomes stay put, whereas in the dynamic one (Movie S2), they move and rotate randomly. KTs are modeled as cylindrical objects and are placed in pairs on opposite sides of the cylindrical surface of the chromosomes, midway along their length (Fig. 1). To simulate the chromosomal MTs, we assume that they are bundled into cylindrical objects extending from the KTs outward, so that the bundle's radius is equal to that of the KT. Therefore, when we model the hybrid centrosomal–chromosomal pathway, we simply consider longer targets placed exactly like the KTs on the chromosomal surface. When a centrosomal MT reaches the chromosomal bundle, we assume that the capture takes place, upon which respective MTs get cross-linked by motors and ultimately establish a K-fiber. Chromosomes continue to move when one or both KTs are captured. Each KT (or extended target) has 10 binding sites on it; as soon as 10 MTs attach to a KT, any next MT that encounters such KT undergoes a catastrophe. Below, we describe additional optional model mechanisms of the error correction. The parameters and technical implementation of the computer simulations are described in Materials and Methods and SI Text.

Results

Chromosome Arms Both Hinder the Search by Shielding KTs and Accelerate the Search by Shortening Unproductive MT Cycles. The first problem one encounters when tens of chromosomes of realistic size are uniformly and randomly distributed within the volume of the nuclear sphere is that the chromosome arms crowd the space to the extent that the chromosomes at the periphery completely shield the KTs in the interior from the MTs protruding from the spindle poles (Fig. 2A). We generated thousands of random chromosome configurations and gathered statistics of the number of the visible KTs (such that a projectile from the pole can reach these KTs without encountering a chromosome arm on the way) (Fig. 2A) and observed that <10% of the KTs can be captured at all if their number is >30. Thus, there has to be a special mechanism that makes all tens of KTs available for the centrosome-guided search.

Next, we tested the assembly process for "smartly" arranged chromosomes: In many configurations, chromosomes were randomly distributed within the nuclear sphere but only special configurations were chosen for testing, so that all KTs were either partially or completely visible from at least one of the centrosomes. Then, the assembly was simulated many times for each such configuration. The resulting average spindle assembly time is presented in Fig. 2B as a function of the KT number and compared with the results of our previous model with transparent chromosome arms (10). For >6 chromosomes, the average assembly time with finite chromosome volume is significantly greater compared with the transparent chromosome model. Moreover, this time increases almost linearly with the number of KTs, much faster than the logarithmic increase predicted by the simplified model (10). The simple explanation for this is that more chromosomes shield a greater fraction of the KT area, so the effective target area decreases with the KT number. This rapidly lengthens the assembly time because more MT cycles are necessary before MT growth in the right direction leads to a capture event.

We noticed, however, that when the chromosome number is small, then the average search time, counterintuitively, decreases when the chromosome arms work as a shield (Fig. 2B Inset). The explanation that we gleaned from following the time-lapse movies of the in silico dynamics is that many MTs growing in the wrong
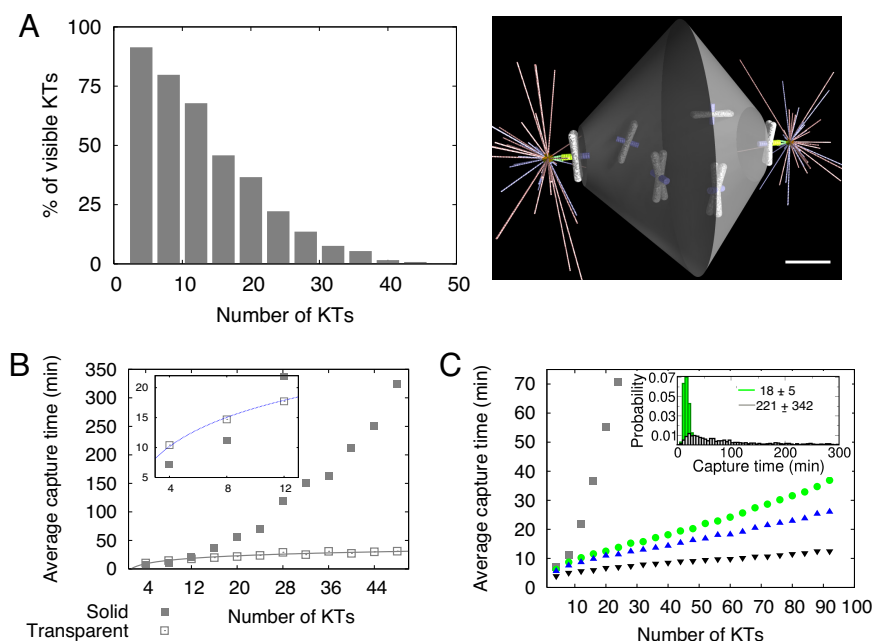
Fig. 2. Effect of the chromosome volume and movements on the assembly speed. (*A*) Chromosomes near the poles shield other chromosomes in the interior of the nuclear sphere from the centrosomal MTs. As a result, the number of KTs "visible" from the spindle poles decreases rapidly as the number of the chromosomes grows. In this and all following figures, the chromosome number is equal to half of the KT number. (Scale bar, 2 μm.) (*B*) Average spindle assembly time (until the last KT is captured) as a function of the KT number with "transparent" (empty squares) and "solid" (shaded squares) chromosome arms. The chromosomes are distributed randomly within the nuclear sphere; only configurations with all KTs at least partially visible were chosen for the searches. The *Inset* shows this function for small KT numbers. (*C*) Computed average capture time as a function of the KT number for static chromosomes (squares) and dynamic, moving chromosomes (circles for $f = 0.005$/sec, upper triangles for $f = 0.01$/sec, lower triangles for $f = 0.1$/sec), where f is the characteristic frequency of a chromosome movement across the nuclear sphere. The *Inset* shows the histograms of the capture times in the unbiased static and dynamic regimes ($f = 0.005$/sec).

direction, not having any KTs in their path, do not waste time on long cycles but, rather, encounter chromosome arms, catastrophe, and get ready to grow in a new direction faster. This observation emphasizes a plausible unexpected role of the chromosome arms in accelerating the assembly by indirectly focusing MTs into the right directions.

Chromosome Movements Accelerate Spindle Assembly. The number of chromosomes in vertebrate cells is much greater than 10, and it is hard to imagine a mechanism able to arrange completely visible static chromosome configurations. However, chromosomes move around the nuclear sphere in prometaphase (25). Characteristic rates of these movements estimated in refs. 26 and 27, where a few microns-per-minute rates of neighbor-independent chromosome movements with frequent changes in direction were reported, suggest that the chromosomes move across the nuclear sphere within hundreds of seconds. In *SI Text*, we report similar data for HT-29 cells, argue that the chromosomes undergo a random walk in the nuclear sphere with similar rates, and discuss physical mechanisms of these movements.

Thus, we assumed in the model that each chromosome moves (jumps to a random location within the nuclear sphere) with characteristic frequency $f \approx 0.001$/sec to 0.1/sec and simulated such jumps (during the movement, chromosomes also reoriented; see further discussion in *SI Text*). Fig. 2*C* shows that the average capture time for dynamic chromosomes moving at frequencies ranging from 0.001/sec to 0.1/sec is order(s) of magnitude shorter than the assembly time in the case of the static chromosomes. Note also that

the dynamic assembly time is not very sensitive to the chromosome number: Random displacements periodically expose each KT to multiple searching MTs, so other chromosomes barely interfere with any given KT capture. Finally, faster (greater frequency) movements decrease the assembly time, but there is the saturation effect. To conclude, chromosome movements drastically accelerate the capture, but still the average spindle assembly time at the observed chromosome mobility is ≈40 min, 3-fold longer than that observed (our data below).

Synergy of Centrosomal and Chromosomal MTs Accelerates Spindle Assembly Further. We propose, following refs. 17 and 28, that the synergy between centrosomal and chromosomal assembly pathways can accelerate spindle assembly: The MT bundle (K-fiber) minus ends growing from the KTs represent greater targets for the dynamic searching centrosomal MTs. The latter encounter and capture the K-fibers by being integrated with the fibers via cross-linking and/or transport mediated by mitotic motors (15, 29). Geometrically, this means an effective increase of the target lengths. We tested the assembly process for various K-fiber lengths and found that the length increase significantly accelerates the capture (Fig. 3*A*): The assembly time is inversely proportional to the K-fiber length, so that just 1-μm-long K-fibers accelerate the capture ≈2-fold compared with 0.3-μm-long KTs, from ≈50 to ≈30 min.

Finally, we found that the spatial bias of the MT dynamics resulting from MTs being stabilized in the nuclear sphere leads to further significant (≈2-fold) reduction of the assembly time (Fig.
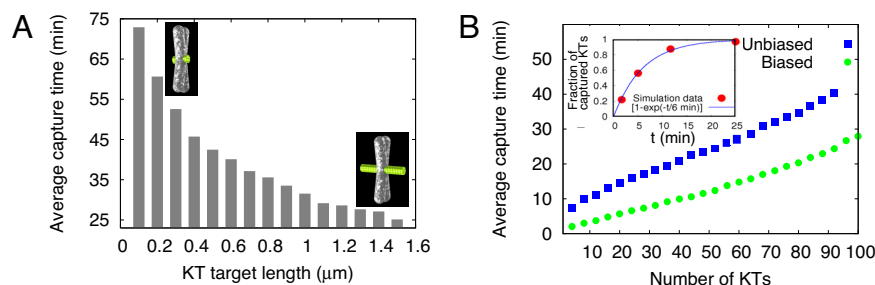
Fig. 3. Effect of chromosomal MTs and biased search on the assembly speed. (*A*) Average capture time for 92 KTs as a function of the target (either KT or chromosomal MT bundle) length. (*B*) Average capture time (for the target length 1 μm) in the unbiased (squares) and biased (circles) pathways. (*Inset*) Fraction of captured KTs as a function of time for 50 chromosomes in the biased search. Circles show the simulation results, and the curve is the exponential fit to the computational data. In *A* and *B*, the chromosomes moved with $f = 0.005$/sec.
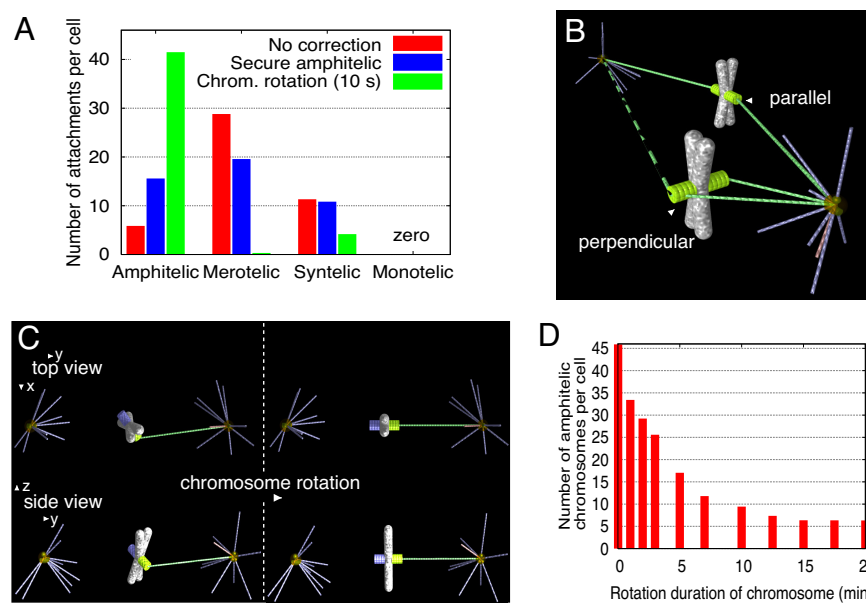
Fig. 4. Error generation and correction mechanisms. (*A*) Numbers of four types of attachments in the biased hybrid searches with 46 dynamic chromosomes (red bars, no correction; blue, amphitelic attachments are secured from further captures; green, chromosomes rotate within 10 sec of the first capture). (*B*) Geometric configurations conducive of the syntelic and amphitelic attachments. Additional attachment (dashed green line) from the distal pole would turn the syntelic attachment into the merotelic one. (*C*) Schematic illustration of the chromosome rotation after the first capture. (*D*) Number of the amphitelic attachments as a function of the rotation duration.

3*B*). Together, the spatial bias of the search and synergy of the centrosomal and chromosomal assembly pathways bring the total assembly time down to ≈20 min for ≈100 KTs. We estimated that HT-29 cells with ≈120 KTs take ≈13–14 min from nuclear envelope breakdown to chromosome alignment at the metaphase plate (Movie S3). It is possible that a few chromosomes may not yet be captured when most of them appear aligned at the metaphase plate. When we plotted the fraction of the captured KTs as a function of time in the biased hybrid search with the dynamic chromosomes (Fig. 3*B Inset*), we observed that the number of captured KTs grows exponentially, so that approximately two-thirds of the chromosomes are captured within just 6 min, and ≈90% are captured in 13 min. Thus, our computational estimate of the assembly time agrees well with the experimental data.

Without Error-Correction Mechanisms, the Majority of Connections in the Spindle Are Erroneous Syntelic and Merotelic Attachments. The swiftness achieved through the synergy of centrosomal and chromosomal MTs, however, comes at a price. When we counted and classified the types of MT-KT attachments for 46 chromosomes, it turned out that ≈30 of the attachments were merotelic, ≈10 were syntelic, and only ≈5 were amphitelic (Fig. 4*A*). This is in contrast with previous observations: Only ≈0.2 chromosomes per cell are syntelically attached in prometaphase PtK1 cells (30), and only ≈30% of prometaphase PtK1 cells possess one or two, very rarely more, merotelically oriented KTs (19).

The reasons for the large predicted number of errors are the following. Once an amphitelic attachment is made, the fully captured chromosome is still "waiting" in the system until all other chromosomes are fully captured. During its waiting period, if all binding sites on its KTs are not occupied, it can still form attachments with new MTs. Sometimes the KT captured from one pole turns and gets exposed to MTs from another pole, so this KT can become merotelically attached. Because the captured chromosomes have to wait longer when the total number of chromosomes is large, the number of merotelic attachments increases with the increasing number of chromosomes. Another reason "gleaned from simulation snapshots" is that because of the crowding of the nuclear sphere, mostly the chromosomes at the periphery, close to the centrosomes, get captured. In agreement with this prediction, the attachments were observed to occur mostly between the chromosomes and proximal pole (31). Such chromosomes very often have both sister KTs visible from the centrosome, so many syntelic

attachments are established rapidly (Fig. 4*B*). Then, additional attachments often turn those into merotelic ones.

Chromosome Rotation After Establishment of the First Attachment Is an Effective Error-Correction Mechanism. We tested a number of plausible error-correction mechanisms. First, we tested the hypothesis that amphitelically attached KTs are secured from any further attachments: Effectively, all binding sites on the captured KT immediately become saturated with MTs from the same pole. The results shown in Fig. 4*A* illustrate that although merotelic attachments are reduced, this does not improve things much: There are still more merotelic attachments than amphitelic ones. The reason is that, as mentioned above, too many syntelic attachments are created in the first place, and those can only remain syntelic or become merotelic (in the model).

This prompted us to consider the idea, widely discussed in the literature (23, 24, 28), that amphitelic attachments are achieved by a process of trial and error, such that syntelic attachments are initially frequent and are dissolved repeatedly (21) until only correct stable attachments survive. Thus, we assumed that syntelic attachments are dissolved within a few seconds upon the second sister KT capture from the same pole, in addition to all amphitelic attachments being secured from any further captures. We found that this mechanism increases the capture time ≈1.5-fold, and still leaves a significant number of merotelic attachments. When, in addition to dissolving the syntelic attachments, we also implemented rapid dissolving of the merotelic connections [when one KT is being captured from both poles; respective preanaphase correction mechanism is discussed in (19, 22)], we were able to almost wipe out all incorrect attachments but at the price of prolonging the assembly process >5-fold. Thus, simply dissolving syntelic and merotelic attachments and starting the search anew improves the accuracy, but hopelessly delays the assembly.

Finally, we tested the elegant idea (23) that a KT target is shielded from the "wrong" pole by the chromosome arms, if the chromosome is oriented properly, with sister KTs facing opposite poles. Based on this idea, we assumed that, upon capture, the chromosome rotates so that the captured KT faces the pole it is captured from, whereas its sister KT faces away from that pole (Fig. 4*C*). The observations that the capture is inefficient when KTs point directly away from the source of properly directed MTs (32) and that proper geometry is important for the capture (33) lend indirect support to this hypothesis. Also, a rapid rotation of the centromere

Fig. 5. Spindle assembly in the presence of an increasing number of spindle poles results in increasing numbers of merotelic KTs. (*A* and *B*) Snapshots of the search-and-capture simulation in a bipolar (*A*) and a tripolar (*B*) spindle. (Scale bars, 2 μm.) (*C*) Predicted (red) and observed numbers (blue) of merotelic attachments in prometaphase cells with two, three, four, and six spindle poles. Because cells with more than four spindle poles are rare, the experimental data for cells with five to eight poles were pooled together in the "Hexapolar" category. The data shown represent means and standard errors (bars). (*D* and *E*) Bipolar (*D*) and tripolar (*E*) prometaphase HT-29 cells immunostained for MTs (green) and KTs (red). Arrowheads point at spindle poles. Images were acquired and processed as described in *Methods* in *SI Text*. (Scale bars, 5 μm.) (*F*) Enlargement of one focal plane from the cell shown in *E*, in which a merotelic KT (boxed area) is visible. A zoomed view of the boxed area in *F* is shown on the right.

was consistently observed just moments before the initiation of chromosome congression (31, 34).

Thus, we propose that after a KT becomes attached to a MT, the chromosome rotates about the point of MT-KT attachment to align the inter-KT axis along the direction of the MT (Fig. 4*C*). In the simulations, during the finite time of the rotation process, the captured and uncaptured KTs are still capable of forming new attachments with the MTs growing from either pole. After the chromosome is fully rotated, the captured KT is geometrically incapable of making further attachments with the other pole. Fig. 4*A* shows the simulation results: This error-prevention mechanism leads to both fast and accurate assembly under the condition that the chromosome rotation takes <10–20 sec (Fig. 4*D*). A few remaining syntelic attachments can be rapidly dissolved, and then the respective chromosomes are likely to be captured accurately without significant delay. We also investigated how the erroneous attachment numbers differ for biased and unbiased searches and for various lengths of the K-fibers and did not see much difference: The growing KT-fibers do not compromise the accuracy because they are shielded from the wrong poles by the chromosome arms, similarly to the KTs. The rotation error-correction mechanism also does not prolong chromosome capture.

Model Correctly Predicts an Increase in Merotelic Attachments in Multipolar Cells. Both older (35) and recent studies (36, 37) showed that higher numbers of merotelic KTs can be found within multipolar spindles, suggesting that spindle geometry might have an effect on establishment of correct vs. incorrect KT attachment. Thus, we set out to test the hypothesis that spindle assembly in the presence of an increasing number of spindle poles would result in an increasing number of KT misattachments (particularly merotelic), because, as previously suggested (36, 37), a single KT would be more likely to face more than one spindle pole within a multipolar spindle compared with a bipolar one, in which the two spindle poles are positioned 180° from each other (Fig. 5 *A* and *B*). Thus, we simulated the search-and-capture process in three-, four- and six-polar spindles. A snapshot of a characteristic tripolar simulation is shown in Fig. 5*B*. In these simulations, we placed the poles at the North and South poles and equator of the nuclear sphere for the three-polar spindle, one additional pole at the opposite side of the equator for the four-polar spindle, and two more poles at the equator, so that four poles at the equator were equidistant, for the six-polar spindle. We also kept the total number of independently

searching MTs constant in all simulations; otherwise, all model parameters were the same as those in the bipolar spindle simulations. These simulations predicted increase of the merotelic attachments per cell from ≈4.2 in the bipolar spindle to ≈4.8, 5.6, and 6.3 in the three-, four-, and six-polar spindles, respectively (Fig. 5*C*).

We next compared the predicted estimates obtained in the simulations with our experimental model of HT-29 cells, which possess ≈60 chromosomes, and in which ≈10% of cells in early prometaphase assemble multipolar spindles (37). We used high-resolution confocal microscopy combined with 3D visualization and image processing (see *Methods* in *SI Text* for details) to identify merotelic KTs in prometaphase HT-29 cells immunostained for KTs and MTs (Fig. 5 *D–F*). We determined the number of merotelic KTs in prometaphases with two, three, four, and five to eight spindle poles (38, 36, 37, and 38 cells, respectively), and found averages of 4.13, 5.08, 5.73, and 6.84 (Fig. 5*C*), respectively. These frequencies are very close to those determined in the simulations (Fig. 5*C*), thus demonstrating the predictive power of our model.

Discussion

We reconstituted in silico the process of mitotic spindle self-assembly in prometaphase, in which hundreds of dynamically unstable MTs grow in random directions and shrink repeatedly until their plus ends encounter KTs, and all chromosomes are thus captured. The chromosomes are crowded into the limited volume of the nuclear sphere, so that the chromosome arms at the periphery shield the KTs of the chromosomes in the nuclear interior. Curiously, the chromosome arms not only hinder the search, but also accelerate it by inducing catastrophes of the wrongly oriented MTs and indirectly focusing the MTs in the right directions. The chromosomes are mobile in prometaphase, and we hypothesize that this mobility is crucial for the assembly speed because it steers the chromosomes exposing all KTs to the searching MTs.

The simulations show that the unbiased MT growth cannot ensure the observed 10- to 20-min-long assembly, but that two factors, acting together, can drastically accelerate prometaphase. The first one—RanGTP-mediated spatial bias of the MT growth into the nuclear sphere (11, 12)—has been investigated earlier (10). The second factor is the synergy of the centrosomal and chromosomal pathway. We found that if astral MTs search for the chromosomal MT bundles growing from the KTs, rather than for the KTs themselves, spindle assembly is faster (10–20 min) because

of the increased size of the effective search targets. This finding predicts that MT ends growing from the KT should be incorporated within the forming mitotic spindle. Indeed, there is increasing evidence that such a pathway contributes to spindle assembly in a number of cell types (7, 29).

However, although the combined centrosomal and chromosomal pathway can speed up the process, it leads to a high number of erroneous attachments, which is in disagreement with observed frequencies of such misattachments in experimental models (19, 30). We also found that securing amphitelic attachments does not fix the problem. We tested, further, whether the widely discussed schematic mechanism of detecting and dissolving the syntelic (and partially merotelic) attachments works and saw that although such mechanism, indeed, "proofreads" the spindle very effectively, it leads to delays of the assembly, so in this case, accuracy comes at the price of speed. Finally, we found that the spindle assembly can be accurate without compromising its speed if, within ≈10–20 sec after the first capture, chromosomes are rotated so that the captured KT faces the pole from which it was captured, and the sister KT becomes shielded from this pole by the chromosome arms. We further discuss the correction and rotation mechanisms and molecular pathways in the *SI Text*.

These conclusions provide quantitative constraints and hypotheses for future studies of mitotic spindle assembly. We calibrated the model using observations of bi- and multipolar colorectal cancer (HT-29) cells. The predictive power of the model is confirmed by the correct predictions of the numbers of the merotelic attachments in bipolar and multipolar HT-29 cells. The model is also in qualitative agreement with recent observations (38) that doubling the chromosome number adds ≈10 min to a ≈20-min cell division. Additional suggestions for future experiments to test the model predictions can be found in *SI Text*.

For clarity, we kept the computational model simple and did not include possible elaborate mechanisms, some reported and other hypothetical, which could significantly accelerate the assembly without compromising the accuracy. For example, we did not consider cooperative chromosome behavior (39, 40). We did not test the possibility of a temporal coordination of the hybrid chromosomal–centrosomal assembly pathway, in which the chromosomal MT bundles growth is delayed relative to the astral MT search (29). More hypothetical mechanisms include clustering of chromosomes or nucleation/branching of nascent MTs off the sides of the K-fibers (41). We discuss relevant issues further in *SI Text*. In the future, when quantitative data on MT and KT dynamics in prometaphase become available, it will not be hard to add and test an impact of these additional mechanisms on the speed and accuracy of the spindle self-assembly.

Materials and Methods

Model Simulations. To simulate the spindle assembly model, we implemented the time-dependent, explicit agent-based simulations (42). In the beginning of each simulation, three classes of objects—chromosomes, KTs (or combined KT–chromosomal bundles), and MTs—were constructed, and then their positions and orientations were changed in the 3D space according to the computational rules described in *Model*, above. Technical details of the simulations and model parameters are described in *SI Text*.

Experimental Observations. The model was calibrated and tested by using colorectal cancer HT-29 cells and by using a number of approaches, including high-resolution confocal microscopy and 3D analysis, phase-contrast time-lapse microscopy, and combined phase-contrast/fluorescence live-cell imaging. The detailed methods are described in *SI Text*.

For additional information, see Figs. S1–S5 and Table S1.

1. Karsenti E, Vernos I (2001) The mitotic spindle: A self-made machine. *Science* 294:543–547.
2. Mitchison TJ, Salmon ED (2001) Mitosis: A history of division. *Nat Cell Biol* 3:E17–E21.
3. Scholey JM, Brust-Mascher I, Mogilner A (2003) Cell division. *Nature* 422:746–752.
4. Kirschner M, Mitchison T (1986) Beyond self-assembly: From microtubules to morphogenesis. *Cell* 45:329–342.
5. Hayden JH, Bowser SS, Rieder CL (1990) Kinetochores capture astral microtubules during chromosome attachment to the mitotic spindle: Direct visualization in live newt lung cells. *J Cell Biol* 111:1039–1045.
6. Rieder CL, Maiato H (2004) Stuck in division or passing through: What happens when cells cannot satisfy the spindle assembly checkpoint. *Dev Cell* 7:637–651.
7. Maiato H, Rieder CL, Khodjakov A (2004) Kinetochore-driven formation of kinetochore fibers contributes to spindle assembly during animal mitosis. *J Cell Biol* 167:831–840.
8. Hill TL (1985) Theoretical problems related to the attachment of microtubules to kinetochores. *Proc Natl Acad Sci USA* 82:4404–4408.
9. Holy TE, Leibler S (1994) Dynamic instability of microtubules as an efficient way to search in space. *Proc Natl Acad Sci USA* 91:5682–5685.
10. Wollman R, et al. (2005) Efficient chromosome capture requires a bias in the "search-and-capture" process during mitotic spindle assembly. *Curr Biol* 15:828–832.
11. Athale CA, et al. (2008) Regulation of microtubule dynamics by reaction cascades around chromosomes. *Science* 322:1243–1247.
12. Bastiaens P, Caudron M, Niethammer P, Karsenti E (2006) Gradients in the self-organization of the mitotic spindle. *Trends Cell Biol* 16:125–134.
13. Varga V, et al. (2006) Yeast kinesin-8 depolymerizes microtubules in a length-dependent manner. *Nat Cell Biol* 8:957–962.
14. Gardner MK, et al. (2008) Chromosome congression by kinesin-5 motor-mediated disassembly of longer kinetochore microtubules. *Cell* 135:894–906.
15. Goshima G, Nedelec F, Vale RD (2005) Mechanisms for focusing mitotic spindle poles by minus end-directed motor proteins. *J Cell Biol* 171:229–240.
16. Heald R, et al. (1996) Self-organization of microtubules into bipolar spindles around artificial chromosomes in *Xenopus* egg extracts. *Nature* 382:420–425.
17. Wadsworth P, Khodjakov A (2004) E pluribus unum: Towards a universal mechanism for spindle assembly. *Trends Cell Biol* 14:413–419.
18. Ault JG, Rieder CL (1992) Chromosome mal-orientation and reorientation during mitosis. *Cell Motil Cytoskeleton* 22:155–159.
19. Cimini D, Moree B, Canman JC, Salmon ED (2003) Merotelic kinetochore orientation occurs frequently during early mitosis in mammalian tissue cells and error correction is achieved by two different mechanisms. *J Cell Sci* 116:4213–4225.
20. Shannon K B, Salmon E (2002) D Chromosome dynamics: New light on Aurora B kinase function. *Curr Biol* 12:R458–R460.
21. Lampson MA, Renduchitala K, Khodjakov A, Kapoor TM (2004) Correcting improper chromosome-spindle attachments during cell division. *Nat Cell Biol* 6:232–237.
22. Cimini D, Wan X, Hirel CB, Salmon ED (2006) Aurora kinase promotes turnover of kinetochore microtubules to reduce chromosome segregation errors. *Curr Biol* 16:1711–1718.
23. Nicklas RB (1997) How cells get the right chromosomes. *Science* 275:632–637.
24. Nicklas RB, Ward SC (1994) Elements of error correction in mitosis: Microtubule capture, release, and tension. *J Cell Biol* 126:1241–1253.
25. Ostergren G, Mole-Bajer J, Bajer A (1960) An interpretation of transport phenomena at mitosis. *Ann NY Acad Sci* 90:381–408.
26. Levesque AA, Compton DA (2001) The chromokinesin Kid is necessary for chromosome arm orientation and oscillation, but not congression, on mitotic spindles. *J Cell Biol* 154:1135–1146.
27. Murata-Hori M, Yu-li Wang YL (2002) The kinase activity of Aurora B is required for kinetochore-microtubule interactions during mitosis. *Curr Biol* 12:894–899.
28. O'Connell CB, Khodjakov AL (2007) Cooperative mechanisms of mitotic spindle formation. *J Cell Sci* 120:1717–1722.
29. Tulu US, Fagerstrom C, Ferenz NP, Wadsworth P (2006) Molecular requirements for kinetochore-associated microtubule formation in mammalian cells. *Curr Biol* 16:536–541.
30. Hauf S, et al. (2003) The small molecule Hesperadin reveals a role for Aurora B in correcting kinetochore–microtubule attachment and in maintaining the spindle assembly checkpoint. *J Cell Biol* 161:281–294.
31. Roos UP (1976) Light and electron microscopy of rat kangaroo cells in mitosis. III. Patterns of chromosome behavior during prometaphase. *Chromosoma* 54:363–385.
32. Rieder CL, Salmon ED (1994) Motile kinetochores and polar ejection forces dictate chromosome position on the vertebrate mitotic spindle. *J Cell Biol* 124:223–233.
33. Loncarek J, et al. (2007) The centromere geometry essential for keeping mitosis error free is controlled by spindle forces. *Nature* 450:745–749.
34. Skibbens RV, Skeen VP, Salmon ED (1993) Directional instability of kinetochore motility during chromosome congression and segregation in mitotic newt lung cells: A push–pull mechanism. *J Cell Biol* 122:859–875.
35. Sluder G, Thompson EA, Miller FJ, Hayes J, Rieder CL (1997) The checkpoint control for anaphase onset does not monitor excess numbers of spindle poles or bipolar spindle symmetry. *J Cell Sci* 110:421–429.
36. Ganem NJ, Godinho SA, Pellman D (2009) A mechanism linking extra centrosomes to chromosomal instability. *Nature* 460:278–282.
37. Silkworth WT, Nardi IK, Scholl LM, Cimini D (2009) Multipolar spindle pole coalescence is a major source of kinetochore mis-attachment and chromosome mis-segregation in cancer cells. *PLoS One* 4(8):e6564.
38. Yang Z, Loncarek J, Khodjakov A, Rieder CL (2008) Extra centrosomes and/or chromosomes prolong mitosis in human cells. *Nat Cell Biol* 10:748–751.
39. Tanaka K, et al. (2005) Molecular mechanisms of kinetochore capture by spindle microtubules. *Nature* 434:987–994.
40. Li Y, Yu W, Liang Y, Zhu X (2007) Kinetochore dynein generates a poleward pulling force to facilitate congression and full chromosome alignment. *Cell Res* 17:701–712.
41. Goshima G, Mayer M, Zhang N, Stuurman N, Vale RD (2008) Augmin: A protein complex required for centrosome-independent microtubule generation within the spindle. *J Cell Biol* 181:421–429.
42. Odell GM, Foe VE (2008) An agent-based model contrasts opposite effects of dynamic and stable microtubules on cleavage furrow positioning. *J Cell Biol* 183:471–483.

Supporting Information

Paul et al. 10.1073/pnas.0908261106

SI Text

Observations of the Chromosome Movements. To quantify the chromosome movements around the nuclear sphere during prometaphase, we used time-lapse microscopy (phase contrast images of the chromosomes and fluorescent KT imaging; see *Methods* below) to track 1–5 chromosomes or KTs in 15 HT-29 cells (33 total chromosomes/KTs tracked) for 2–4 min at 30-sec intervals (Fig. S1) and established that individual chromosomes in prometaphase moved at a rate of ≈1.5 μm/min. Directions of displacement of one chromosome in consecutive 30-sec intervals were correlated, but the correlation was lost in the second 30-sec-long time interval. These estimates suggest that the chromosomes undergo a random walk characterized by the effective diffusion coefficient that can be estimated as $D \approx v^2 t/3$ (1), where $v \approx 1.5$ μm/min is the chromosome speed within a short interval, and $t \approx 50$ sec is the average time between drastic direction changes. Thus, the effective diffusion coefficient is $D \approx 0.01$ μm^2/sec. The characteristic time, T, needed for a chromosome to move across the nuclear sphere as a result of this random walk can be estimated as $T R_{\mathrm{nuc}}^2/6D \approx 15$ μm^2/0.06 μm^2/sec ≈ 250 sec. Similar data can be extracted from the KT tracking. We also observed that the mean square displacement of the tracked KTs increases linearly with time, so that ≈10 μm^2 displacement takes place in ≈150 sec, in agreement with the chromosome tracking. These observations agree with the published estimates cited in the main text. Future systematic measurements will be needed to collect enough statistics of tracking more chromosomes/KTs per cell for longer time to obtain more precise characteristics of the chromosome movements in prometaphase.

Mechanisms of Chromosome Movements and Rotations and MT–Chromosome Interactions. The chromosome movements can be due to three processes acting in parallel: (*i*) MTs pushing on the chromosome arms through the polymerization force (2); (*ii*) MTs pushing on the chromosome arms through interaction with molecular motors on the chromosome arms (3); thermal Brownian motion. The MTs approach the arms from the wide range of angles, so the first two mechanisms will also result in an effective Brownian motion of the chromosomes. In principle, simple polymerization ratchet forces of growing MTs would be sufficient to push the chromosomes around (2). However, there is ample data showing that in prometaphase, dynein/dynactin (4, 5), CENP-E (5, 6) and chromokinesin (reviewed in ref. 7) are involved in chromosome movements. Likely, minus-end-directed dynein is responsible for the poleward motion, whereas plus-end-directed chromokinesin on the chromosome arms accounts for the antipoleward "wind" (8). Another less prominent but distinct possibility is that the actin cytoskeleton, either directly (9) or via nuclear myosin-I-mediated transport (10), is responsible for chromosome movement.

Similarly, the hypothesized chromosome rotations after the first capture can be driven by a combination of the motor-generated and MT polymerization ratchet forces. The initial low-tension attachment is likely to lead to KT-attached MT depolymerization (11, 12), which will exert a net torque on the respective chromosome to reorient to be aligned with the spindle axis. In addition, dynein motors could drive monooriented KTs poleward (13, 14, 15). There were reports that Calyculin A, myosin enhancer, causes prometaphase chromosomes to move rapidly up and back along the spindle axis, and to rotate (16). Finally, chromosome rotations can be chromokinesin dependent

(8, 17). Monotelic chromosomes are often oriented in a "V" shape with the captured KTs pulled poleward and their arms pushed away from the pole (17). This observation suggests that the pulling of the captured KT toward the respective pole (contribution of dynein) combined with the pushing on the chromosome arms by astral MTs (contribution of chromokinesin) can rotate the chromosome in the desired orientation.

We based the assumption that a MT starts to shorten immediately upon a contact with a chromosome arm on the following results: in vitro, growing MTs were observed to catastrophe rapidly upon running into a wall (18). The authors of this study concluded that the polymerization force upon the impact shortened the time before the catastrophe. Similarly, in vivo, a number of studies established that growing MTs catastrophe rapidly upon encountering cell membrane (19), cell cortex (where MTs interacted transiently with dyneins) (20), and spindle pole bodies (21). Extrapolating these results, we assume that MTs also catastrophe upon a contact with a chromosome arm. Importantly, there are a few seconds of active physical contact before this catastrophe (18). During this short time interval the MTs plus ends can push the chromosomes directly or through interactions with chromokinesin motors. Multiple pN-range pushing for brief time intervals can easily account for the chromosome movements. In the computational model, the fastest characteristic process during the spindle assembly has the time scale of 10 seconds, so for computational purposes we can safely assume that MTs shorten immediately upon a contact with a chromosome arm.

Notes on the Simulations of the Chromosome Movements. Without experimental indications to the contrary, we make the simplest assumption that the chromosomes do the random walk with self-avoidance (there are steric interactions between the chromosomes preventing them from physical overlapping). In the crowded environment of the nuclear sphere, accurate 3D computer simulations of such walk are very computationally expensive (22). Besides, the following ambiguities remain: Some simulations predict anomalous subdiffusion, whereas others result in normal diffusion, and available experimental results usually disagree with these simulations (reviewed in ref. 22). Thus, in the absence of rigorous established algorithm, we settled on the simplest numerical procedure: We estimated a finite time interval over which, according to extrapolated estimates from experimental observations, a chromosome is displaced over distances comparable with the size of the nuclear sphere. Then, each such time interval, we displace the chromosome to a random location within the sphere, and then "jiggle" it locally until it does not overlap with any other chromosomes. In principle, a more accurate simulation would be to reduce the time interval, to scale down the average displacement (as the square root of the time interval), and to displace the chromosomes over small distances and time intervals jiggling them every time to avoid overlaps. Unfortunately, we discovered that systematic exploration of the model regimes and parameters in 3D with such small steps becomes prohibitive, even on a computer cluster. However, we tested this more accurate algorithm for one of the search scenarios (biased, with chromosome rotation, with certain fixed parameters) for time intervals between the chromosomal jumps equal to 5, 10, 20, and 200 sec (respective average displacements are 1.1, 1.5, 2.2, and 7 μm). The results (Figs. S2 and S3) illustrate that the model predictions are not very sensitive to the reduction of the time step. However, indeed,

it seems that the more accurate procedure does predict a faster (by ≈15%) and slightly more accurate (also by ≈15%) assembly. The differences in the results start to become evident for short time intervals of ≈5–10 sec, and because of computer limitations, we cannot explore them further at the present.

Because we are not yet able to trace the chromosomes over long time intervals, we cannot ascertain that they indeed perform an unbiased random walk. Indeed, in the future it may well become clear that the chromosome movements are less random and more correlated and/or undergo more localized, confined walk than we assume. However, even in this case, our current model will provide necessary null hypothesis to check against. In the future, we plan to explore further both precise biological mechanisms of chromosome movements, and simulations of those.

Molecular Mechanisms of the Error Correction. It is a good idea to add complexity to the model gradually, in steps, each time obtaining an insight of how the next level of complexity changes the model predictions. Including more molecular details at this stage would diffuse valuable lessons. For this reason, we did not explicitly model molecular mechanisms of the error correction and chromosome turning, because our goal in this article was to obtain quantitative mechanistic insight into the geometry and kinetics of spindle self-assembly. However, the data presented here constitutes the groundwork for future studies aimed at elucidating the roles of complex protein networks in maintaining the timing and faithfulness of mitosis. In this respect, it is worthwhile to consider principal molecular players of the error correction mechanisms.

In recent years, experimental work led to the identification of some of the key proteins involved in correction of KT misattachment. For example, Ipl1/Aurora B kinase, required for proper biorientation of chromosomes (23), was shown to destabilize syntelic KT attachments in both yeast (24, 25) and vertebrate cells (26). In addition, Aurora B has also been shown to play a role in correction of merotelic attachments (27). Similarly, the kinesin-13 MCAK appears to be involved in correction of both syntelic and merotelic attachments (28). The fact that Aurora B regulates the MT de-stabilizer MCAK (28, 29) and that this regulation is tension dependent (30) provides further support for Aurora B's role in error correction mechanisms. Likely, the list of proteins involved in misattachment correction is still incomplete. Future modeling efforts will use currently available data, such as rates of KT-MT turnover with and without Aurora B kinase activity (31), to help identify other still unknown key components of this protein network responsible for error correction.

Discussion of Some Mechanisms That Can Affect the Speed and Accuracy of Prometaphase. There were reports that monooriented chromosomes initially move toward the pole to which they first attach (reviewed in ref. 32). This could increase the number of KT attachments to the correct pole at the initially captured KT. It will also lead to the hypothesized reorientation of the KTs. After this initial movement, the chromosome could be gliding back toward the spindle equator alongside KT fibers attached to other already bioriented chromosomes (6). We simulated numerically this initial poleward movement allowing the chromosome to stay at 2 μm from the respective pole for 100–200 sec, after which the chromosome started to move again. We discovered that this additional mechanism indeed increased the accuracy of the assembly, but delayed the assembly a fewfold.

Another pathway alternative to the chromosomal one is that MCAK in the centromeric region promotes catastrophe of MT plus ends passing by that region, which might end up as merotelic attachments (33). Effectively, this means increasing the chromosomal radius in the KT vicinity. Trial runs of the model with

such feature indicated that this mechanism, indeed, can improve the accuracy with only minor effect on the assembly speed.

It is possible that some MTs running into the chromosome arms do not catastrophe, but instead are guided (presumably by motors) along the arms toward the respective KTs or that the MTs can even go through or around the arms. We simulated the scenario in which a certain percentage (30% to 50%) of MTs was not affected by their interactions with the chromosome arms. As a result, the speed of assembly increased slightly, whereas the accuracy worsened: number of syntelic and merotelic attachments grew in proportion to the number of MTs passing through the arms.

It is not out of question that the "poleward wind" generated by the pushing astral MTs crowds the chromosomes to the spindle equator. What effect would this have on spindle assembly? We tested this scenario computationally and found that such crowding would not compromise the accuracy, but would actually prolong the assembly 1.5-fold. Also, it is interesting to note that whereas a normal human cell has 23 pairs of chromosomes (i.e., 46 chromosomes and 92 KTs), the aneuploid cancer HT-29 cells have the greater number of ≈50–60 chromosomes. According to our simulations, fewer chromosomes are captured slightly faster more accurately. Indeed, KT misattachments in PtK1 cells (n = 12) occur at lower frequencies (34) than those found in HT-29 cells (N ≈ 60; (35) and this study)). Also, mitosis in normal diploid cells is predicted to be faster and more accurate than in aneuploid cancer cells, providing that the other kinetics do not change.

Finally, multiple error correction mechanisms are likely to operate during the prometaphase. We tested the scenario in which the chromosomes both rotate after the first capture, syntelic attachments are corrected. In this case, the average capture time increase is negligible, whereas accuracy significantly improves—almost 99% of attachments become amphitelic.

Suggestions for Future Experiments to Test the Model Predictions. (*i*) Accurate tracking of the chromosome movements in 3D can be done with the help of marking chromosome arms by using in vivo visualization based on lac repressor recognition of direct repeats of the lac operator (36). (*ii*) The model predicts that there will almost always be a chromosomal rotation before biorientation, so after the rotation there will be a capture from the opposite pole and movement. This prediction can be tested with tracking one of available kinetochore markers. (*iii*) To see whether the chromosome movement facilitates the biorientation, one can use both tracking kinetochores (with a standard kinetochore marker) and by using a fluorescence resonance energy transfer-based biosensor that can sense the activity of Aurora-B. This activity is shown to correlate with biorientation (30), so one would be able to test whether the chromosomes moving around more/faster also bipolarize more quickly. (*iv*) The model predicts that chromokinesin inhibition should lengthen the time necessary for spindle assembly and perhaps perturb chromosome rotation. This could be tested by using siRNA technique to inhibit function of various chromokinesin motors. (*v*) Some cells (for example, mouse cells) have only telocentric chromosomes (i.e., chromosomes that have only one arm, in other words they are V-shaped rather than X-shaped, with the KT at one end, and the two sister chromatids extending away from the centromere/KT only in one direction, Figs. S4 and S5). We simulated the search-and-capture in such cells (Figs. S4 and S5) and found that, with chromosome number, volume, and other model parameters being the same, the speed and accuracy of the spindle assembly in such cells are the same as in the cells with metacentric (investigated in this article) chromosomes. This prediction can be tested by measuring the prometaphase duration and number of merotelic attachments in mouse cells.

Methods. *Model simulations.* (*i*) To save computational time and avoid the difficulty of tracking steric interchromosomal interactions, we did not move the chromosomes in the dynamic scenario continuously, but rather moved each chromosome once every $1/f$ seconds, where f is the movement frequency, to a random location within the nuclear sphere, at the same time with rotating the chromosomes randomly. Immediately after that, the chromosomes are "jiggled" locally to avoid overlapping between them. (*ii*) MT dynamics were simulated by the Monte Carlo algorithm: A random number was generated between 0 and 1 with equal probability. At each computational step (with time increment $\Delta t = 1$ sec) MT switches to shortening if this random number is less than $(1 - f_{cat} \times \Delta t)$. (*iii*) All computational data were obtained from running simulations for each set of parameters 500 times. (*iv*) The numerical codes were implemented with C programming language. Numerical experiments were performed on an IBM dual CPU Opteron server.

The model parameters given in Table S1 were chosen from the following considerations. The MT number and four dynamic instability parameters (ν_g, ν_s, $f_{ca[infi]t}$, f_{res}) are of the same orders of magnitude as respective parameters reported and discussed in (37, 38, 39). We made the MT growth and shortening rates twice faster than those in ref. 38, which is plausible. The chromosome number, size of the nuclear sphere and KT size came from our observations (see *Methods*); KT number is twice the chromosome number. The orders of magnitude of the length and radius of the chromosomes were reported in refs. 40 and 41. The characteristic time, T, needed for a chromosome to move across the nuclear sphere is estimated from the literature and observations reported above as hundreds of seconds. In the final simulations, we used the value of the frequency of random jumps around the nuclear sphere $f \approx 1/(200 \text{ sec})$, varied this frequency two orders of magnitude around this value.

Experimental observations. Cell culture. HT-29 cells (American Type Culture Collection) were maintained in McCoy's 5a medium (Gibco) complemented with 10% FBS, penicillin, streptomycin, and amphotericin B (antimycotic) and grown in 5% CO_2 in a humidified incubator kept at 37 °C. For experiments, cells were grown on sterile coverslips inside 35-mm Petri dishes.

Immunostaining. Cells were first incubated in ice-cold medium for 10 min at 4 °C. Next, cells were rapidly rinsed in PBS, fixed in 4% formaldehyde, and then permeabilized for 10 min in PHEM buffer containing 0.5% Triton X-100. Subsequently, cells were rinsed in PBS, and then blocked in 10% boiled goat serum for 1 h at room temperature. The coverslips were then incubated in primary antibodies: CREST (human anti-centromere protein; Antibodies Inc.) diluted 1:100 and mouse anti-α-tubulin (DM1A; Sigma–Aldrich) diluted 1:500 in 5% boiled goat serum overnight at 4 °C. Cells were then rinsed in PBST (PBS with 0.05% Tween 20), incubated in secondary antibodies (X-Rhodamine goat-anti-human; Jackson ImmunoResearch Laboratories, Inc., diluted 1:100, and Alexa Fluor 488 goat-anti-mouse; Molecular Probes, diluted 1:400) for 1 h at room temperature, rinsed again, and mounted in an antifade solution containing 90% glycerol and 0.5% N-propyl gallate.

Immunofluorescence microscopy and image analysis. Immunofluorescently stained cells were imaged with a Swept Field Confocal system (Prairie Technologies) on a Nikon Eclipse TE2000-U inverted microscope. The microscope was equipped with a 100 × 1.4 N.A. Plan-Apochromatic phase-contrast objective lens, phase-contrast transillumination, transmitted light shutter, and ProScan automated stage (Prior Scientific). The confocal was equipped with filters for illumination at 488 or 568

nm from a 400-mW argon laser and a 150-mW krypton laser. Digital images were acquired with an HQ2 CCD camera (Photometrics). Image acquisition, shutter, z axis focus, laser lines, and confocal system were all controlled by NIS Elements AR (Nikon) software on a PC computer. Z-series optical sections through each imaged cell were acquired at 0.6-μm steps. Linear measurements were performed by using the two-point length measurement tool in NIS Elements AR. The size of 22 KTs in each of five cells was measured after determining the best focal plane for each one of them. To measure the mitotic nuclear sphere (i.e., volume through which chromosomes were distributed in prometaphase cells), two perpendicular measurements were taken in the *XY* plane, followed by two perpendicular measurements taken at 45° rotation from the first two. Finally, the chromosome sphere thickness was measured along the cell z axis. The number of merotelic attachments in prometaphase cells was determined by analyzing the acquired images in multiple ways. First, both the KT and MT images were processed through the special filtering function of NIS Elements to increase the contrast. These two processed images were then merged and smoothed by using the smooth function of NIS Elements. Merotelically attached KTs were then identified by scrolling along the z axis to visualize KTs bound to MT bundles oriented in opposite directions. When a merotelic KT was identified, a "ratio view" (NIS Elements function) was also created for that specific focal plane. This view allowed the identification of regions of juxtaposition between a KT and its MT bundle(s). All of the differently processed views of the image were simultaneously analyzed to exclude all of the cases in which a MT bundle ran past a KT rather than ending on it.

Live-cell imaging. Coverslips at $\approx$70% confluency were mounted into a Rose chamber without top coverslip. The chamber was filled with L-15 medium with 4.5 g/L glucose, and mineral oil was added on top to prevent evaporation. Experiments were performed on a Nikon Eclipse TE2000-U inverted microscope equipped with phase contrast transillumination, transmitted light shutter, ProScan automated stage (Prior Scientific), Lumen 200PRO Fluorescence Illumination system, and HQ2 CCD camera (Photometrics). Cells were maintained at $\approx$36 °C by means of an air stream stage incubator (Nevtek). Images were acquired and analyzed through the NIS Elements AR software. For prometaphase timing, images of 10 different fields of view were acquired at 30-sec min intervals over a 3-h period with a 20× objective, and the experiment was repeated five5 times. The time-lapse movies were subsequently analyzed to identify cells undergoing mitosis during the period of recording. Prometaphase timing was calculated as the time elapsed between nuclear envelope breakdown (NEB) and chromosome alignment at the metaphase plate. For prometaphase chromosome dynamics, phase-contrast images of 15–20 different fields of view were acquired at one focal plane every 30 sec over a 4-h period with a 100× 1.4 N.A. Plan-Apochromatic phase contrast objective. The experiment was repeated twice. Cells entering mitosis were subsequently identified in the time-lapse movies, and chromosomes were manually tracked for 4–10 consecutive frames. To confirm the phase contrast chromosome tracking, one experiment was performed in cells transiently transfected with pmTagRFP-T-CENPB-N-22 vector (a generous gift from M. Davidson, Florida State University, Tallahassee) by using a Nucleofector Device (Lonza). The transfected cells were grown on coverslips up to $\approx$70% confluency before observation. Coverslips were mounted in sealed Rose chambers filled with phenol red-free L-15 medium supplemented with 4.5g/L glucose.

1. Berg HC (1993) *Random Walks in Biology* (Princeton Univ Press, Princeton).
2. Dogterom M, Kerssemakers JW, Romet-Lemonne G, Janson ME (2005) Force generation by dynamic microtubules. *Curr Opin Cell Biol* 17:67–74.
3. Brouhard GJ, Hunt AJ (2005) Microtubule movements on the arms of mitotic chromosomes: Polar ejection forces quantified in vitro. *Proc Natl Acad Sci USA* 102:13903–13908.

4. Vorozhko VV, Emanuele MJ, Kallio MJ, Stukenberg PT, Gorbsky GJ (2008) Multiple mechanisms of chromosome movement in vertebrate cells mediated through the Ndc80 complex and dynein/dynactin. *Chromosoma* 117:169–179.

5. Murata-Hori M, Yu-li Wang YL (2002) The kinase activity of Aurora B is required for kinetochore–microtubule interactions during mitosis. *Curr Biol* 12:894–899.

6. Kapoor TM, et al. (2006) Chromosomes can congress to the metaphase plate before biorientation. *Science* 311:388–391.

7. Mazumdar M, Misteli T (2005) Chromokinesins: Multitalented players in mitosis. *Trends Cell Biol* 15:349–355.

8. Rieder CL, Salmon ED (1994) Motile kinetochores and polar ejection forces dictate chromosome position on the vertebrate mitotic spindle. *J Cell Biol* 124:223–233.

9. Lénárt P, et al. (2005) A contractile nuclear actin network drives chromosome congression in Oocytes. *Nature* 436:812–818.

10. Chuang C-H, et al. (2006) Long-range directional movement of an interphase chromosome site. *Curr Biol* 16:825–831.

11. Gardner MK, et al. (2005) Tension-dependent regulation of microtubule dynamics at kinetochores can explain metaphase congression in yeast. *Mol Biol Cell* 16:3764–3775.

12. Franck AD, et al. (2007) Tension applied through the Dam1 complex promotes microtubule elongation providing a direct mechanism for length control in mitosis. *Nat Cell Biol* 9:832–837.

13. Yang Z, Tulu US, Wadsworth P, Rieder CL (2007) Kinetochore dynein is required for chromosome motion and congression independent of the spindle checkpoint. *Curr Biol* 17:973–980.

14. Varma D, Monzo P, Stehman SA, Vallee RB (2008) Direct role of dynein motor in stable kinetochore–microtubule attachment, orientation, and alignment. *J Cell Biol* 182:1045–1054.

15. Gassmann R, et al. (2008) A new mechanism controlling kinetochore–microtubule interactions revealed by comparison of two dynein-targeting components: SPDL-1 and the Rod/Zwilch/Zw10 complex. *Genes Dev* 22:2385–2399.

16. Fabian L, Troscianczuk J, Forer A (2007) Calyculin A, an enhancer of myosin, speeds up anaphase chromosome movement. *Cell Chromosome* 6:1–9.

17. Levesque AA, Compton DA (2001) The chromokinesin Kid is necessary for chromosome arm orientation and oscillation, but not congression, on mitotic spindles. *J Cell Biol* 154:1135–1146.

18. Janson ME, de Dood ME, Dogterom M (2003) Dynamic instability of microtubules is regulated by force. *J Cell Biol* 161:1029–1034.

19. Tran PT, Marsh L, Doye V, Inoué S, Chang F (2001) A mechanism for nuclear positioning in fission yeast based on microtubule pushing. *J Cell Biol* 153:397–411.

20. Kozlowski C, Srayko M, Nedelec F (2007) Cortical microtubule contacts position the spindle in *C. elegans* embryos. *Cell* 129:499–510.

21. Tischer C, Brunner D, Dogterom M (2009) Force- and kinesin-8-dependent effects in the spatial regulation of fission yeast microtubule dynamics. *Mol Syst Biol* 5:250–257.

22. Dix JA, Verkman AS (2008) Crowding effects on diffusion in solutions and cells. *Annu Rev Biophys* 37:247–263.

23. Hauf S, et al. (2007) Aurora controls sister kinetochore mono-orientation and homolog bi-orientation in meiosis-I. *EMBO J* 26:4475–4486.

24. Biggins S, Murray AW (2001) The budding yeast protein kinase Ipl1/Aurora allows the absence of tension to activate the spindle checkpoint. *Genes Dev* 15:3118–3129.

25. Tanaka Tet al. (2002) Evidence that the Ipl1-Sli15 (Auora kinase-INCENP) complex promotes chromosome bi-orientation by altering kinetochore–spindle pole connections. *Cell* 108:317–327.

26. Hauf S, et al. (2003) The small molecule Hesperadin reveals a role for Aurora B in correcting kinetochore-microtubule attachment and in maintaining the spindle assembly checkpoint. *J Cell Biol* 161:281–294.

27. DeLuca JG, et al. (2006) Kinetochore microtubule dynamics and attachment stability are regulated by Hec1. *Cell* 127:969–982.

28. Kline-Smith SL, Khodjakov A, Hergert P, Walczak CE (2004) Depletion of centromeric MCAK leads to chromosome congression and segregation defects due to improper kinetochore attachments. *Mol Biol Cell* 15:1146–1159.

29. Knowlton AL, Lan W, Stukenberg PT (2006) Aurora B is enriched at merotelic attachment sites, where it regulates MCAK. *Curr Biol* 16:1705–1710.

30. Liu D, Vader G, Vromans MJ, Lampson MA, Lens SM (2009) Sensing chromosome bi-orientation by spatial separation of aurora B kinase from kinetochore substrates. *Science* 323:1350–1353.

31. Cimini D, Wan X, Hirel CB, Salmon ED (2006) Aurora kinase promotes turnover of kinetochore microtubules to reduce chromosome segregation errors. *Curr Biol* 16:1711–1718.

32. Rieder CL, Salmon ED (1998) The vertebrate cell kinetochore and its roles during mitosis. *Trends Cell Biol* 8:310–318.

33. Ohi R, Coughlin ML, Lane WS, Mitchison TJ (2003) An inner centromere protein that stimulates the microtubule depolymerizing activity of a KinI kinesin. *Dev Cell* 5:309–321.

34. Cimini D, Moree B, Canman JC, Salmon ED (2003) Merotelic kinetochore orientation occurs frequently during early mitosis in mammalian tissue cells and error correction is achieved by two different mechanisms. *J Cell Sci* 116:4213–4225.

35. Silkworth WT, Nardi IK, Scholl LM, Cimini D (2009) Multipolar spindle pole coalescence is a major source of kinetochore mis-attachment and chromosome mis-segregation in cancer cells. *PLoS One* 4(8):e6564.

36. Belmont AS, Straight AF (1998) In vivo visualization of chromosomes using lac operator-repressor binding. *Trends Cell Biol* 8:121–124.

37. Maiato H, Rieder CL, Khodjakov A (2004) Kinetochore-driven formation of kinetochore fibers contributes to spindle assembly during animal mitosis. *J Cell Biol* 167:831–840.

38. Wollman R, et al. (2005) Efficient chromosome capture requires a bias in the ''Search-and-Capture'' process during mitotic spindle assembly. *Curr Biol* 15:828–832.

39. Tulu US, Fagerstrom C, Ferenz NP, Wadsworth P (2006) Molecular requirements for kinetochore-associated microtubule formation in mammalian cells. *Curr Biol* 16:536–541.

40. Harrison CJ, Allen TD, Britch M, Harris R (1982) High-resolution scanning electron microscopy of human metaphase chromosomes. *J Cell Sci* 56:409–422.

41. Sumner AT (1991) Scanning electron microscopy of mammalian chromosomes from prophase to telophase. *Chromosoma* 100:410–418.
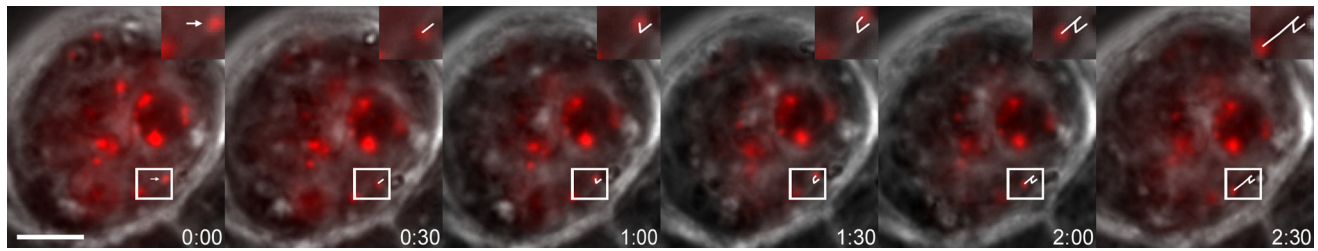
Fig. S1. Chromosome movements. Still images from a time-lapse movie of HT-29 prometaphase cell transfected with mTagRFP-T-CENPB. Phase-contrast images of the cell were merged with the fluorescent images of the KTs (red). The *Inset* at the top right corner of each frame shows a 200% enlargement of the boxed area. The arrow in the first *Inset* points at a KT that was tracked during the experiment. A track of KT movement over time was overlaid to the images (white lines in the boxed areas and insets). The kinetochore tracked here moved at a rate of 1.2 μm/min. Elapsed time shown in min:sec. (Scale bar, 5 μm.)
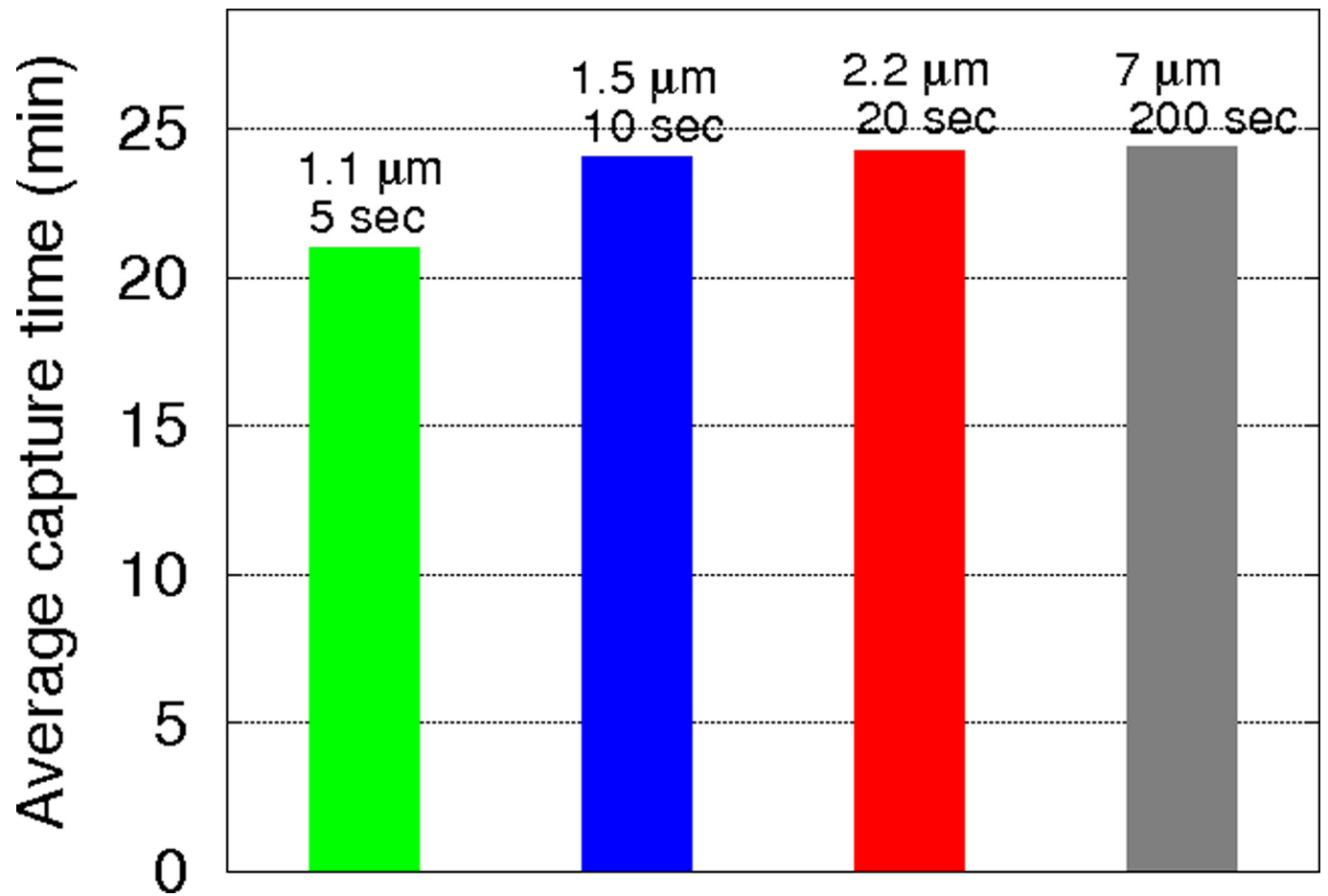
Fig. S2. Capture time for more detailed simulations of the chromosomal movements. Results of computer simulations in which the chromosomes were moved in random direction by normally distributed average distance over short time intervals (the time intervals and average distances were scaled so that the effective diffusion coefficient remained constant) and then jiggled locally every time to avoid overlaps. The capture time is not very sensitive to the fine-graining of the movements. The chromosomes rotated within 10 sec after the first capture.
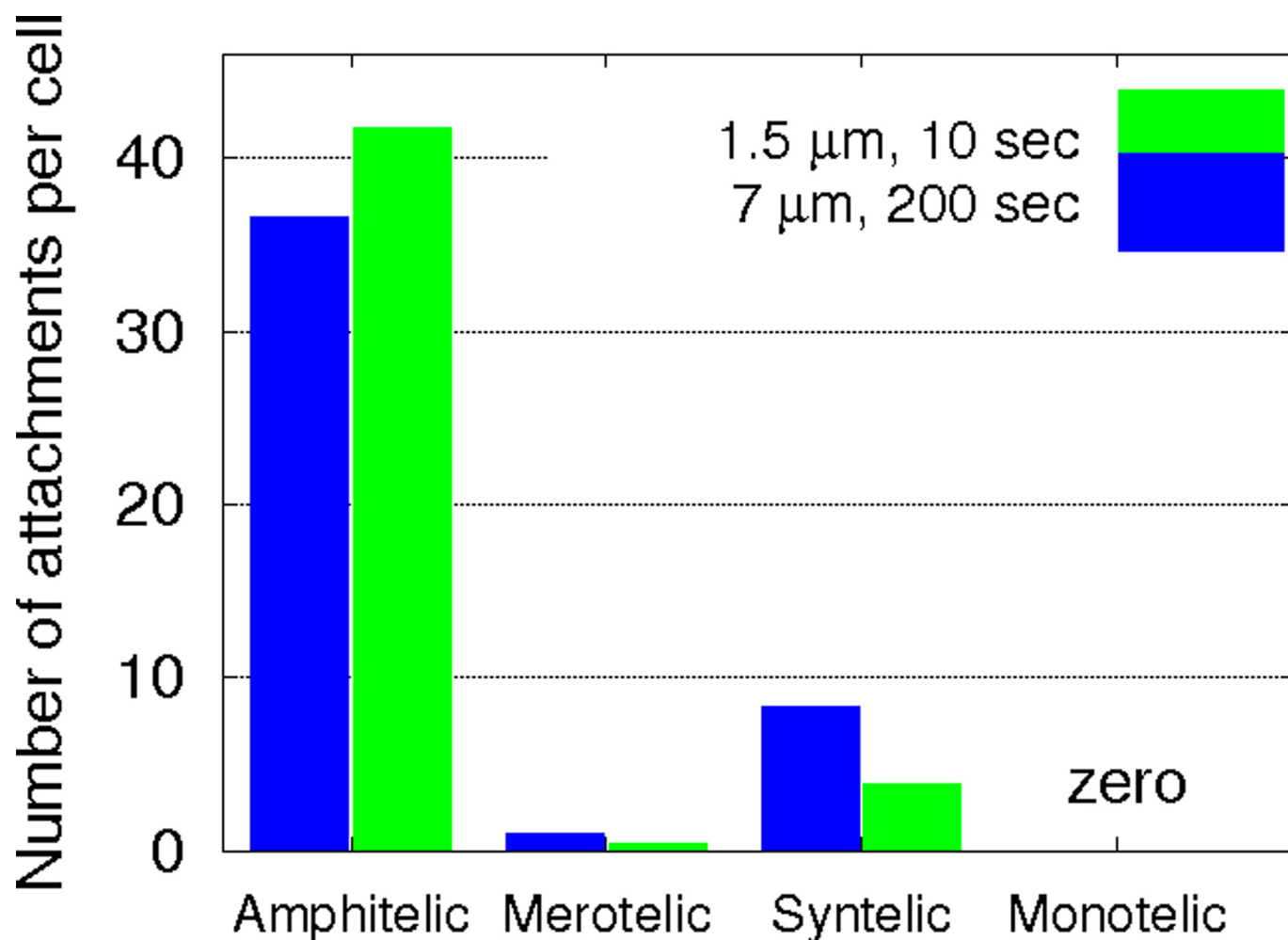
Fig. S3. Numbers of four distinct attachments for more detailed simulations of the chromosomal movements. Results of computer simulations in which the chromosomes were moved in random direction by normally distributed average distance over short time intervals (the time intervals and average distances were scaled so that the effective diffusion coefficient remained constant), and then jiggled locally every time to avoid overlaps. Results for only two (short and long) time intervals are shown; for intermediate time intervals, the numbers of attachments are intermediate between those shown. The amphitelic and merotelic attachment numbers are not very sensitive to the fine-graining of the movements. The chromosomes rotated within 10 sec after the first capture.
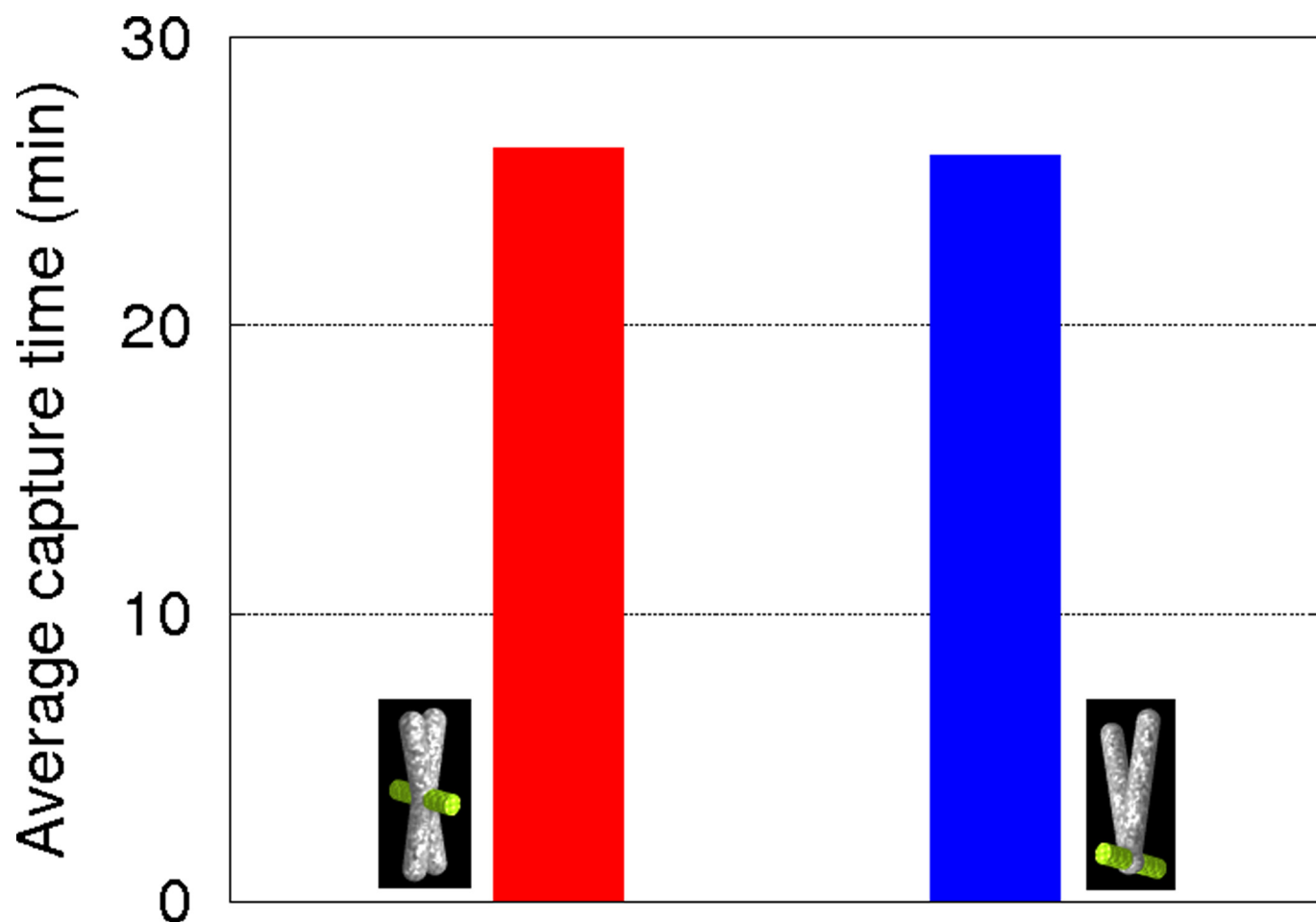
Fig. S4. Capture time in cells with metacentric and telocentric chromosomes. The results are obtained from simulations with chromosome number, volume, and other model parameters being the same for both types of chromosomes.
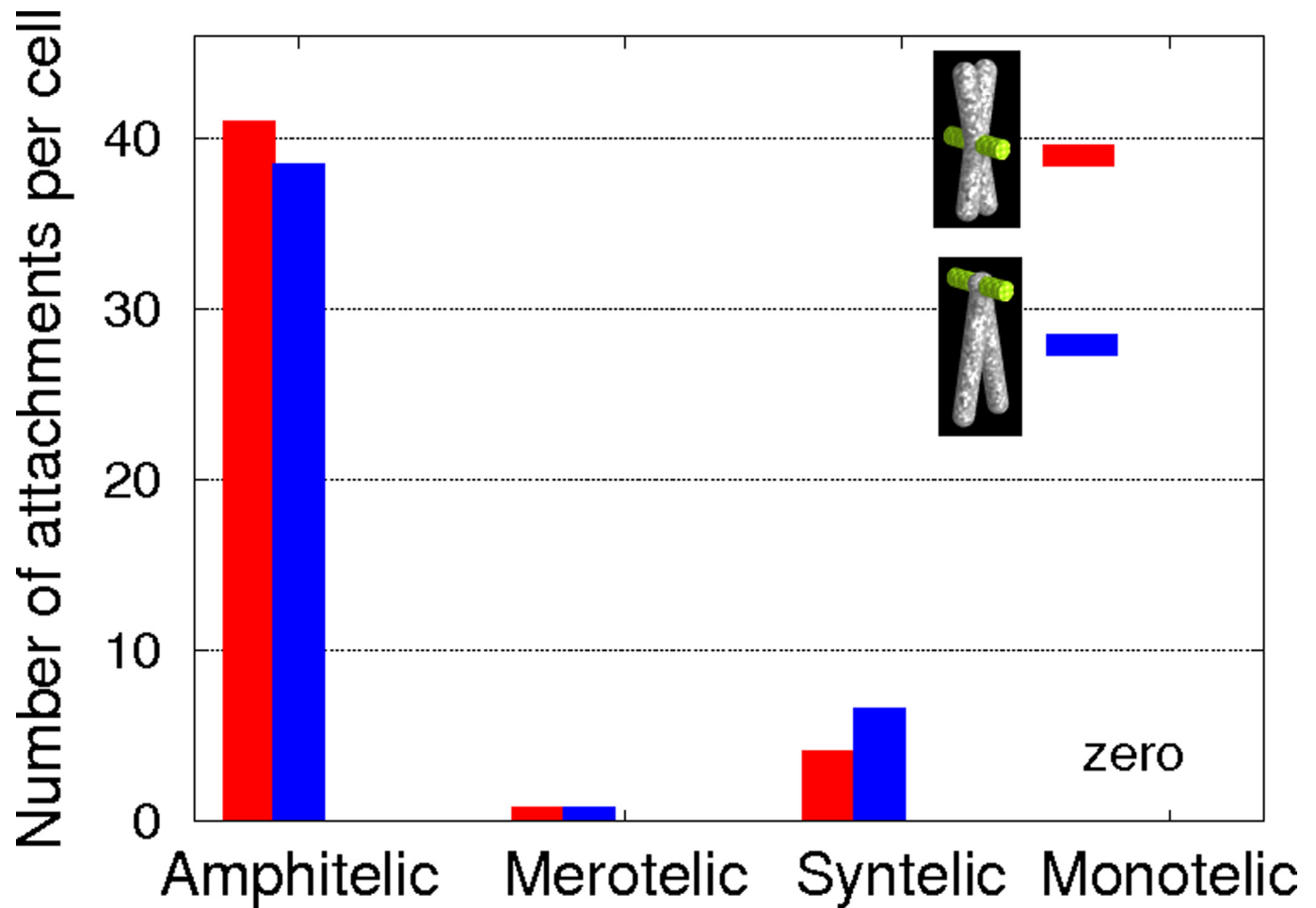
Fig. S5. Numbers of four distinct attachments in cells with metacentric and telocentric chromosomes. The results are obtained from simulations with chromosome number, volume, and other model parameters being the same for both types of chromosomes.

Table S1. Model parameters

| Symbol	Description	Value
N_{CH}	Chromosome number in the simulations	1–50
N_{KT}	KT number in the simulations	2–100
N_{MT}	Number of dynamic MTs at each pole	250
R_{CH}	Chromosome radius	1 μm
R_{KT}	KT radius	0.44 μm
l_{CH}	Chromosome length	2 μm
l_{KT}	Target (KT or K-fiber) length	0.1–1.5 μm
R_{nuc}	Radius of the nuclear sphere	7 μm
ν_g	MT growth rate	0.35 μm/sec
ν_s	MT shortening rate	1 μm/sec
F_{cat}	Catastrophe frequency in the unbiased search	$3\nu_g/4R_{nuc} \approx 0.04$/sec
f_{res}	Rescue frequency	0
τ	Chromosome rotation time after the capture	1–200 sec
f	Frequency of chromosomal movements across the nuclear sphere	0.001–0.1/sec
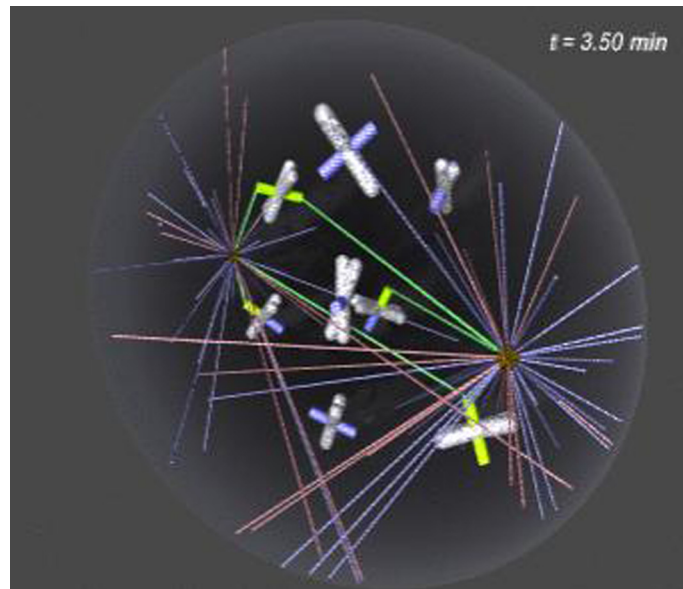
Movie 1. Time-lapse time movies of the computer search and capture simulation with static chromosomes. Growing MTs are blue, shortening MTs are red, captured MTs are green; captured KTs are green, not captured KTs are blue.

Movie S1 (WMV)
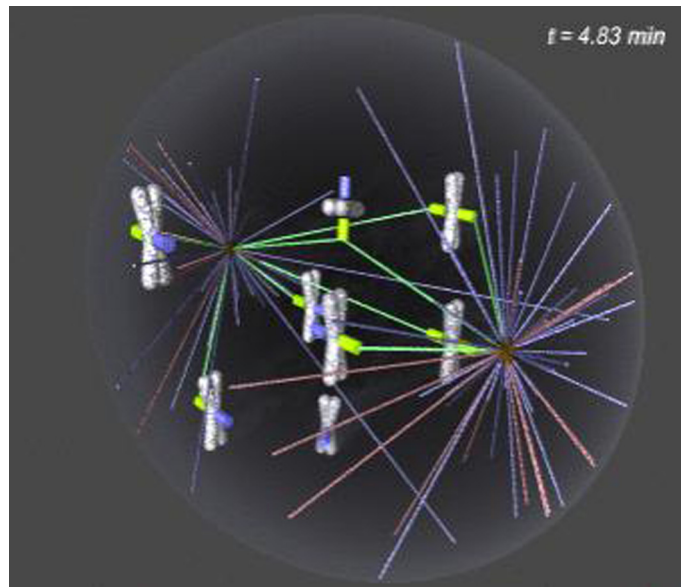
Movie S2. Time-lapse time movies of the computer search and capture simulation with dynamic chromosomes. Growing MTs are blue, shortening MTs are red, captured MTs are green; captured KTs are green, not captured KTs are blue.

Movie S2 (WMV)
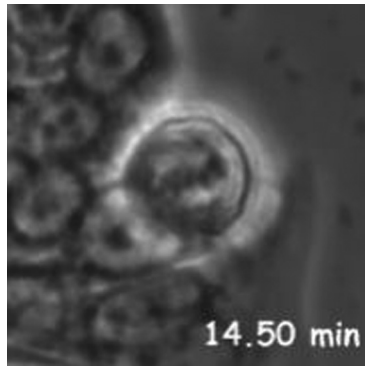
Movie S3. Time-lapse movie of HT-29 cell entering mitosis and aligning its chromosomes at the metaphase plate. The cell is in interphase when the movie starts, but it rounds up and enters mitosis at 7 min. The movie ends when the cell completes chromosome alignment at the metaphase plate (20:50). Elapsed time shown in min:sec.

[Movie S3 (AVI)](#)